

# DESIGN OF INPUT COUPLER FOR RIKEN SUPERCONDUCTING QUARTER-WAVELENGTH RESONATOR

K. Ozeki<sup>#</sup>, O. Kamigaito, H. Okuno, N. Sakamoto, K. Suda, Y. Watanabe, K. Yamada,  
 RIKEN Nishina Center, Saitama, Japan  
 E. Kako, H. Nakai, K. Umemori,  
 High Energy Accelerator Research Organization (KEK), Ibaraki, Japan  
 K. Okihira, K. Sennyu, T. Yanagisawa,  
 Mitsubishi Heavy Industries Ltd. (MHI), Hiroshima, Japan

## Abstract

An accelerator system based on the superconducting quarter-wavelength resonator is being constructed at the RIKEN Nishina Center. As part of the conceptual design of the input coupler, the optimal positions of the cold window and the thermal anchor were discussed according to the residual resistivity ratio of copper plating. We report on the details of that discussion.

## INTRODUCTION

At the RIKEN Nishina Center, construction of an accelerator system based on the superconducting quarter-wavelength resonator (QWR) is underway with the goal of developing basic technologies for the superconducting linear accelerator for ions. A cryomodule that can mount two QWRs is now being constructed as a prototype [1]. In this system, cryocoolers for a helium recondenser and a thermal shield were considered in order to achieve a system that does not require large refrigerators. Cooling power for the recondenser is assumed to be 6 W per resonator, which can be realized by three GM/JT cryocoolers (CG310SLCR). A single thermal shield is installed and cooled to 40 K using a single-stage cryocooler. Many kinds of cryocoolers are available for cooling the thermal shield. The assumed cooling power for the thermal shield is about 90 W.

Characteristics of the input coupler are as follows: The resonance frequency of the cavity is 75.5 MHz and assumed beam loading is about 1 kW. The assumed maximum RF power is 10 kW. Disk-type double vacuum windows are adopted. The cold window is set at the vicinity of the thermal anchor. To reduce thermal conduction from the external portion, the inner and outer conductors are fabricated from 1-mm-thick copper-plated stainless steel.

Reference [2] reports significant reduction in the residual resistivity ratio (RRR) of copper plating on stainless steel due to heat treatment. At higher RRR, dynamic loss decreases and thermal conduction increases, while at lower RRR dynamic loss increases and thermal conduction decreases. As part of the conceptual design of the input coupler, the optimal positions of the thermal anchor and the cold window were discussed, based on estimations of thermal conduction and dynamic losses, in which constant thickness and various RRRs of the copper

plating were assumed. Because the skin depth of the room-temperature copper is about 15 μm, the thickness of the copper plating was assumed to be 20 μm.

## THERMAL AND ELECTRICAL CONDUCTIVITIES

The thermal conductivities of copper for various RRRs were obtained from Refs. [3] and [4]. The top panel of Fig. 1 shows the thermal conductivities of the copper for RRR = 5, 10, 30, and 100. An imaginary thermal conductivity for RRR = 1 is also shown. These thermal conductivities were converted to electrical conductivities (bottom graph in Fig. 1) using the Wiedemann–Franz law:

$$\sigma = \frac{K}{LT},$$

where  $K$  and  $\sigma$  are the thermal and electrical conductivities,  $T$  is temperature, and  $L$  is the Lorenz

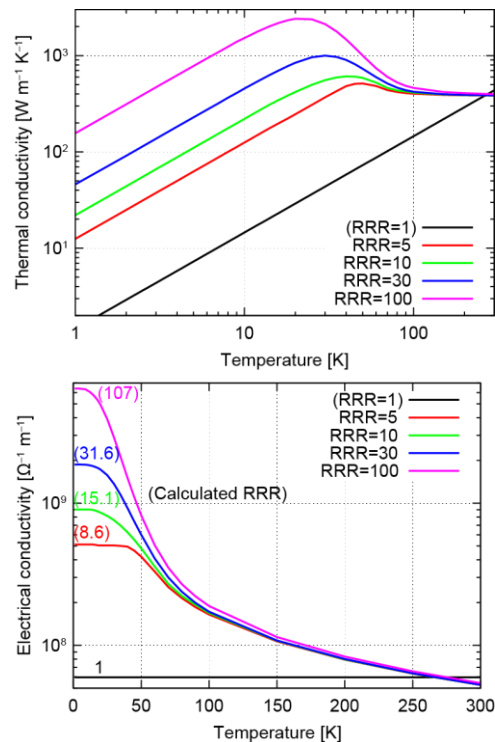


Figure 1: (top) Thermal conductivities of copper for various RRRs. (bottom) Electrical conductivities of copper derived from the thermal conductivities. Calculated RRRs are shown for each curve.

<sup>#</sup>k\_ozeki@riken.jp

number. The value of the Lorenz number used here is a theoretical value of  $2.44 \times 10^{-8} \text{ W } \Omega \text{ K}^{-2}$ . The RRRs obtained from these curves are shown in the bottom panel of Fig. 1, and differ slightly from the nominal values (e.g., for the nominal RRR of 100, the obtained RRR is 107). Therefore, the electrical conductivities of copper for RRR = 2, 5, 10, 20, 30, 50, 70, and 100 were artificially created by interpolating five curves of the electrical conductivities, including an imaginary RRR = 1 (top panel of Fig. 2). These electrical conductivities were again converted to thermal conductivities using the Wiedemann–Franz law (bottom panel of Fig. 2). Thermal conduction and dynamic losses were estimated using these conductivities.

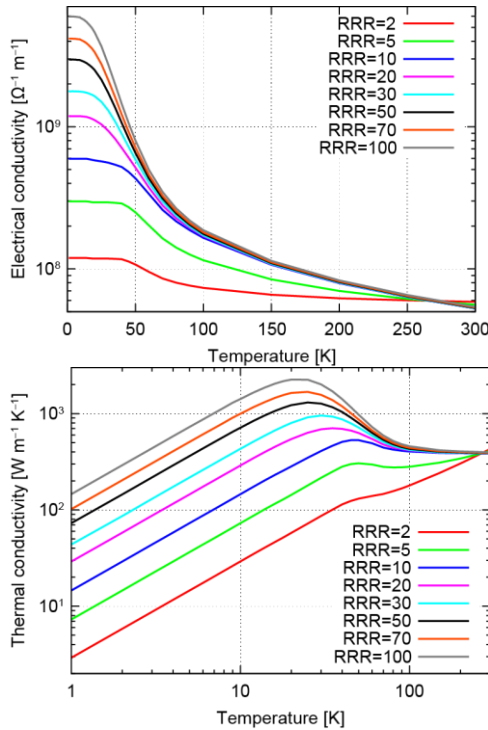


Figure 2: (top) Electrical conductivities artificially constructed by interpolating the curves in Fig. 1. (bottom) Thermal conductivities derived from the artificial electrical conductivities.

### MECHANICAL DESIGN OF INPUT COUPLER

Figure 3 shows the structure of the input coupler assumed in this study. The bellows were appropriately allocated to compensate for displacement due to the low temperature and reduction of thermal conduction. Table 1 lists the configurations of each bellows (circled numbers in Fig. 3). The temperature of the cold window was assumed to be a constant 40 K. In the following estimations, the position of the cold window is expressed as the distance from the taper part of the coupler, as shown in Fig. 3.

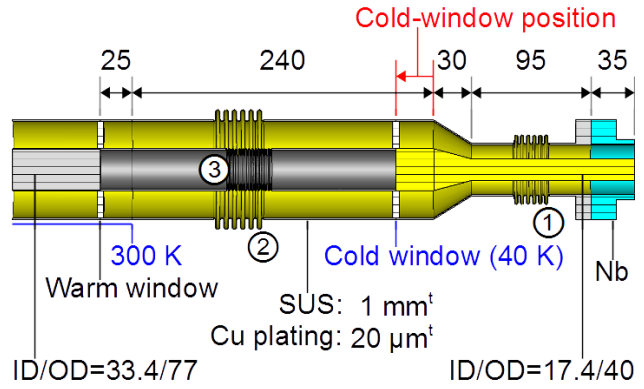


Figure 3: Input coupler structure.

Table 1: Bellows Configurations

Bellows #	1	2	3
ID [mm]	41	77	22.5
OD [mm]	55	95	33
Pitch $P$ [mm]	4.8	6.6	2.6
Thickness $t$ [mm]	0.15	0.15	0.15
Convolutions	6	6	14

### ESTIMATION OF THERMAL CONDUCTIONS

Table 2 summarizes the thermal conductivities averaged over two temperature regions, 4.2–40 K and 40–300 K. The bellows were approximated by the shape shown in Fig. 4. The temperature difference  $\Delta T$  for one convolution of the bellows is obtained as

$$\Delta T = \frac{Q \cdot P/2}{2\pi r_o t K} + \frac{Q \cdot P/2}{2\pi r_i t K} + 2 \int_{r_i}^{r_o} \frac{Q}{2\pi r t K} dr,$$

where  $P$  is the pitch of the bellows,  $r_o = \text{OD} - P/8$ ,  $r_i = \text{ID} + P/8$ ,  $Q$  is the heat quantity,  $K$  is the thermal conductivity, and  $t$  is the thickness of the bellows or copper plating. Thermal conduction into the cavity and the thermal anchor were estimated for various RRRs. As an example, Fig. 5 shows the thermal conduction estimated for RRR = 30.

Table 2: Thermal Conductivities Averaged Over Each Temperature Region [ $\text{W m}^{-1} \text{K}^{-1}$ ]

RRR	4.2–40 K	40–300 K
2	64	268
5	158	329
10	303	405
20	522	420
30	735	431
50	1046	445
70	1345	457
100	1796	477

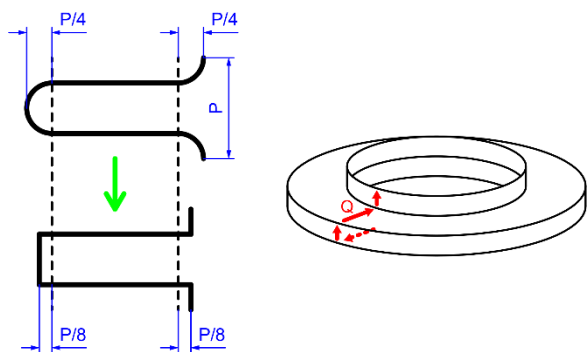


Figure 4: Approximated shape of bellows.

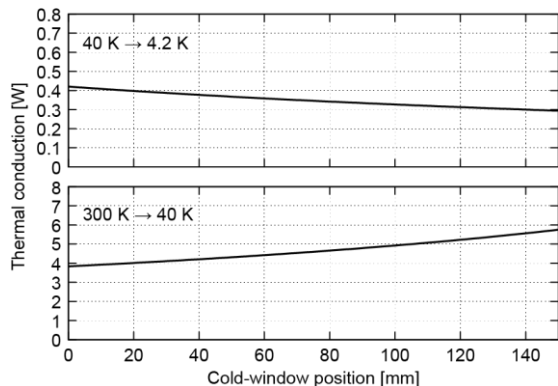


Figure 5: Thermal conduction into cavity and thermal anchor as a function of cold-window position estimated for RRR = 30.

### ESTIMATION OF DYNAMIC LOSSES

The dynamic losses for various RRRs were estimated based on computations using CST Microwave Studio [5]. When computing RF power losses, the input coupler was segmented, and the temperature of each segment was assumed as shown in Fig. 6. To be on the safe side, the temperatures were set a little higher, so dynamic losses were also estimated to be a little higher. The head of the inner conductor was set to be 50 K, considering the temperature increase due to RF power loss. Table 3 summarizes the electrical conductivities at each temperature for various RRRs. For the traveling wave, RF power losses at each segment were computed as a function of the cold-window position. Figure 7 shows an example of the computation. The computed RF power losses were scaled to stimulated RF powers of 1, 5, and 10 kW. Figure 8 shows the dynamic losses at each part estimated for RRR = 30.

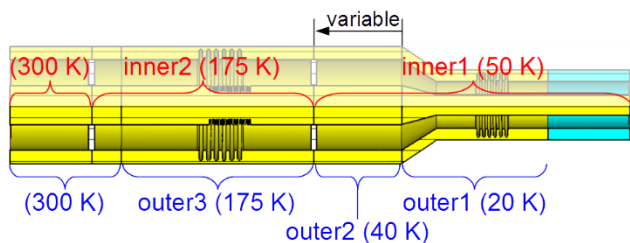


Figure 6: Input coupler configuration for computing RF power losses.

Table 3: Adopted Electrical Conductivities [ $\Omega^{-1} \text{ m}^{-1}$ ]

RRR	20 K	40 K	50 K	175 K
2	$1.2 \times 10^8$	$1.2 \times 10^8$	$1.1 \times 10^8$	$6.4 \times 10^7$
5	$2.9 \times 10^8$	$2.9 \times 10^8$	$2.5 \times 10^8$	$7.7 \times 10^7$
10	$5.8 \times 10^8$	$5.2 \times 10^8$	$4.3 \times 10^8$	$9.3 \times 10^7$
20	$1.1 \times 10^9$	$7.1 \times 10^8$	$5.2 \times 10^8$	$9.4 \times 10^7$
30	$1.6 \times 10^9$	$8.9 \times 10^8$	$5.9 \times 10^8$	$9.4 \times 10^7$
50	$2.5 \times 10^9$	$1.1 \times 10^9$	$6.5 \times 10^8$	$9.5 \times 10^7$
70	$3.4 \times 10^9$	$1.2 \times 10^9$	$7.1 \times 10^8$	$9.7 \times 10^7$
100	$4.6 \times 10^9$	$1.4 \times 10^9$	$8.0 \times 10^8$	$9.8 \times 10^7$

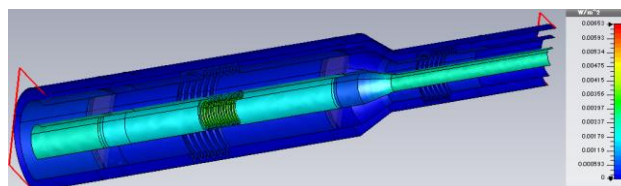


Figure 7: Example of computed RF power loss distribution for RRR = 30. Stimulated RF power is 0.5 W. Cold-window position is 25 mm.

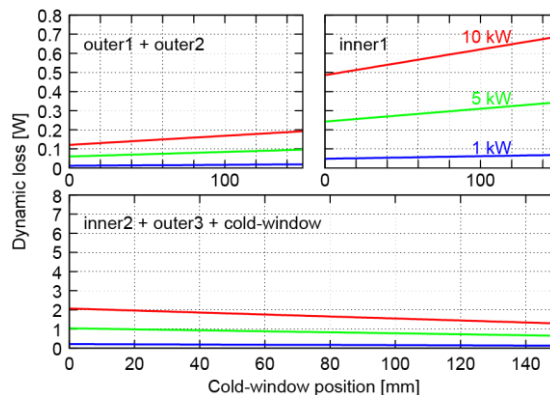


Figure 8: Dynamic losses at each part as a function of cold-window position estimated for RRR = 30.

### HEAT FLOWS INTO CAVITY AND THERMAL ANCHOR

In Fig. 8, dynamic loss denoted by “outer1 + outer2” flows into the cavity. Heat flow into the cavity is represented as the sum of the dynamic loss at this part and the thermal conduction, denoted by “40 K → 4.2 K”. In contrast, the dynamic losses denoted by “inner1” and “inner2 + outer3 + cold window” flow into the thermal anchor. Heat flow into the thermal anchor is represented as the sum of the dynamic losses at these parts and the thermal conduction, denoted by “300 K → 40 K”. Figure 9 shows heat flows into the cavity and the thermal anchor for RRR = 30. The curves denoted by “0 kW” (black) correspond to the static heat flow according to the thermal conduction shown in Fig. 5.

#### Optimal Cold-window Position

To determine the optimal position of the cold window, we formulated the following function (the “window-position function,” below) as a figure of merit:

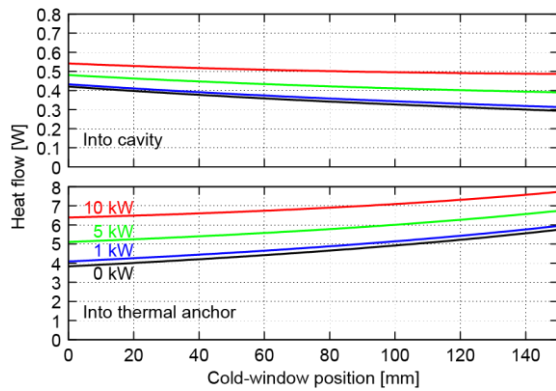


Figure 9: Heat flows into the cavity and thermal anchor as a function of cold-window position estimated for RRR=30.

$$F_{wp} = \frac{\text{Heat flow into cavity}}{\text{Admissible heat flow into cavity}} + \frac{\text{Heat flow into thermal anchor}}{\text{Admissible heat flow into thermal anchor}}$$

Based on heat flow estimation with a cryomodule other than the input coupler [1], the admissible heat flows into the cavity and the thermal anchor were estimated to be 1.3 W and 35 W, respectively. In this case, the window-position function was obtained by summing the flows in the top panel of Fig. 9 (denoted by “Into cavity”) normalized by 1.3 and the flows in the bottom panel of Fig. 9 (denoted by “Into thermal anchor”) normalized by 35. Figure 10 shows the result. The minimum position of the curve for a stimulated RF power of 10 kW was defined as the optimal position (about 80 mm). Figure 12 shows heat flows into the cavity and the thermal anchor, as well as the window-position functions for various RRRs. It was found that the cold window should be placed at a position close to the cavity for lower RRR, and at a position distant from the cavity for higher RRR.

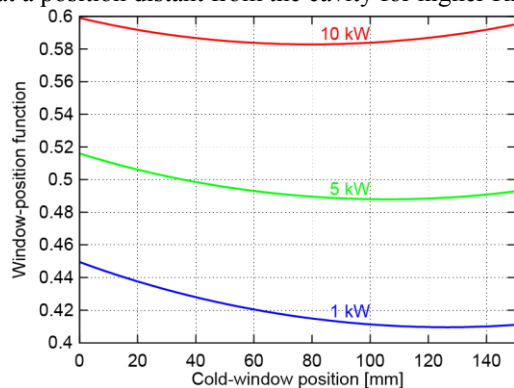


Figure 10: Window-position function for RRR = 30.

The heat flows into the cavity shown in Fig. 12 suggest that the RRR of copper should have a value between 5 and 20, if it is adjustable, because heat flow into the cavity is minimized for RRR in this range. However, the RRR of copper used for the head of the inner conductor

(the part corresponding to “inner1” in Fig. 6) should be kept high, because this part is involved in only dynamic loss, not thermal conduction from the external portion.

### TEMPERATURE INCREASE AT HEAD OF INNER CONDUCTOR

Temperature increase at the head of the inner conductor was estimated in order to evaluate the necessity of a cooling system for the head of the inner conductor. Figure 11 shows a model for estimation of the temperature increase at the head of the inner conductor. The assumed RRR of copper was 70. The parameters  $Q_{tc}$ ,  $Q_{rad}$ , and  $Q_{rf}$  represent the heat flow by thermal conduction, the heat flow by thermal radiation, and the RF power loss on the surface of the inner conductor, respectively. The thermal radiation was negligibly small compared with the other heat quantities. As a result of the estimation, we concluded that the cooling system was unnecessary.

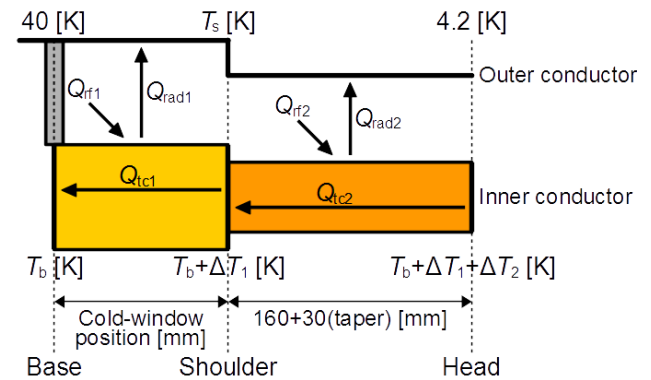


Figure 11: Model for estimation of temperature increase at head of inner conductor.

### SUMMARY

The positions of the thermal anchor and the cold window were discussed as part of the conceptual design of the input coupler for the RIKEN superconducting QWR. Estimations of the heat flows into the cavity and the thermal anchor for various RRRs of copper plating suggested that a relatively low RRR is preferable, and the positions of the cold window and the thermal anchor should be close to the cavity.

### ACKNOWLEDGMENT

This work was funded by ImPACT Program of Council for Science, Technology and Innovation (Cabinet Office, Government of Japan).

### REFERENCES

- [1] N. Sakamoto, et al., in these proceedings, WEBA06.
- [2] K. Kanaoka et al., Proc. of ERL2015, WEICLH2062.
- [3] <http://tpds.db.aist.go.jp/tpds-web/>.
- [4] <http://cryogenics.nist.gov/>.
- [5] <https://www.cst.com/Products/CSTMWS/>.

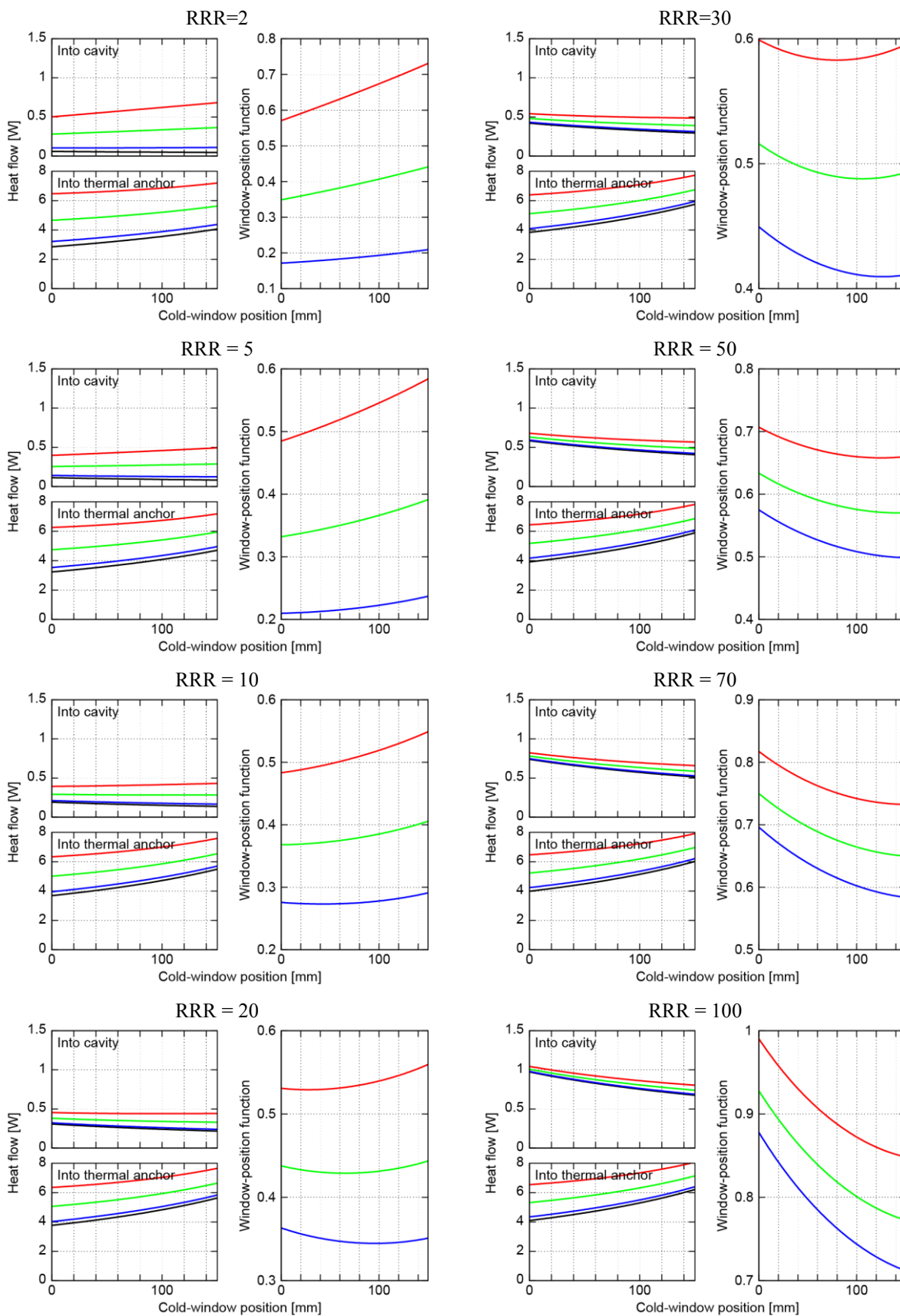


Figure 12: Heat flows into cavity and thermal anchor, and window-position functions for various RRRs. Black, blue, green, and red curves correspond to stimulated RF powers of 0, 1, 5, and 10 kW, respectively.